Analyzing and Interpreting NMR Spin–Spin Coupling Constants Using Molecular Orbital Calculations

Jochen Autschbach* and Boris Le Guennic
Department of Chemistry, State University of New York at Buffalo, Buffalo, NY 14260–3000; **jochena@buffalo.edu*

The pedagogical value of computational chemistry in the chemistry curriculum, in particular the value of first-principles calculations of NMR chemical shifts *(1, 2),* has been previously pointed out in this *Journal.* Emphasis has been put on providing recipes for addressing well-defined problems computationally and on comparing experimental with calculated data. These are important ingredients that can enable students to support their future (usually experimental) graduate research projects with their own calculations, to get a feeling about the accuracy that can be achieved, and to be able to assess the quality of published theoretical data. Quantum chemistry is now a component of many graduate research projects. Introducing students to the power and the limitations of quantum chemical methods, and to the theoretical background, is therefore an important aspect of a modern chemistry education.

NMR spectroscopy is one of the most important experimental techniques since it is able to provide useful information about the electronic and geometric structures of a wide variety of systems investigated in organic and inorganic chemistry. Additionally, theoretical methods have been used extensively to compute chemical shifts and spin–spin coupling constants from first-principles theory. (See refs *3–10* for a selection of available review articles.) A comprehensive overview of computational methods for magnetic resonance parameters has also recently become available *(11).* With the help of calculations, it is possible to simulate NMR spectra, propose data for yet unknown substances, get detailed insight into the mechanisms that determine the experimental outcome, and so forth.

Indirect NMR spin–spin coupling constants, also known as *J* coupling constants, provide a wealth of structural information as well as detailed insight into the bonding of an atom to its neighbors. In this article, we show how density functional theory (DFT) calculations of *J* couplings can help to clarify the relation between such properties and the electronic structure and bonding in molecules. This is achieved by the analysis of *J* coupling in terms of contributions from molecular orbitals (MOs), localized molecular orbitals (LMOs), and fragment orbitals (FOs). We should point out that such analyses for organic *(12–17)* and inorganic systems *(18–22)* are also an active research topic. Here, we apply an orbital analysis to one-bond carbon–carbon coupling, J(C,C), in ethane, ethene, and ethyne. The C−C coupling constants in the aromatic molecule benzene as well as C−H couplings for all molecules are also discussed. We show how a graphically-oriented approach, combined with "hard" numerical data, can lead to a better understanding of the nature of *J* coupling and of the orbital description of the electronic structure of molecules. In addition, we use the concept of *localized molecular orbitals* and apply it to rationalize the magnitudes of the C−C coupling constants. Unlike the "usual" MOs, these orbitals are the theoretical equivalent of the bonds and lone pairs (and core shells) of the Lewis formula of a molecule. Unfortunately, they are not prominently displayed in most textbooks.

To the best of our knowledge, NMR spin–spin coupling computations and orbital analyses based thereupon have not yet been discussed in this *Journal.* We believe that the material will be most useful in a course about NMR spectroscopy or as a computational exercise as part of a computational chemistry or molecular modeling course. It is now possible to compute NMR spin–spin coupling constants rather accurately with inexpensive DFT methods. This makes a study of small molecules attractive for use in a classroom or for homework. We hope that this article will be beneficial to a wider range of courses since the concepts used here can be applied to analyze other properties as well (see Appendix A, Table 8, in the Supplemental Material[W] for a list of such properties). A computational analysis of trends in *J* couplings might also be suitable as a computational undergraduate or graduate research project (e.g., if applied to a different set of molecules). Course prerequisites depend on the level at which an instructor teaches a particular course. Introductory physics and some basic knowledge of NMR spectroscopy as acquired in undergraduate organic chemistry classes will be essential. A qualitative explanation of *J* coupling at this level is given in the first half of the second section. Basic quantum theory as taught in undergraduate physical chemistry courses will be required to make use of the quantum theory of *J* coupling, which is outlined in the Appendix in the Supplemental Material.[W] This theory supports the arguments regarding the s character of bonds presented in the second half of the second section. However, more qualitative explanations might be chosen instead. We do not think that prior experience with computational chemistry is necessary for the calculations presented in the third section, though of course it would be helpful. Based on these calculations, we apply various analysis concepts to the *J* coupling in ethane, ethene, ethyne, and benzene in the third section. Here, we make use of molecular orbital plots. Some experience with qualitative molecular orbital theory will be required to use these graphics.

Origin and Mechanisms of *J* Coupling

For further details regarding the material presented in this section we refer to refs *23* and *24.*

Magnetic Dipole Moments

Moving charged particles (electrons, nuclei) represent an electric current, which is the source of a magnetic field. In particular, electric *ring currents* are the source of a magnetic field equivalent to that of a magnetic dipole (Figure 1). In turn, a magnetic field will induce electric ring currents[1] with an associated magnetic dipole moment in a system of charged particles (atoms, molecules).

When considering a single rotating charged particle, the magnetic moment **m** is proportional to its angular momentum **L**. The constant of proportionality is the magnetogyric ratio γ, that is, $\mathbf{m} = \gamma\mathbf{L}$. For instance, for the orbital rotational motion of an electron, we have $\gamma_e = -e/(2m_e)$, where e is the electronic charge and m_e is the mass of the electron.

Spin and Magnetic Moment

The property "spin" is an angular momentum of an elementary particle. Spin is often incorrectly interpreted as the particle's intrinsic rotation. However, according to the previous paragraph this analogy from classical physics illustrates why there must be a magnetic moment associated with the spin angular momentum of a charged particle. Atomic nuclei with an odd mass number or with an odd number of neutrons have a nuclear spin angular momentum (usually labeled **I**, not **L**). Thus, nuclei with nonzero spin are tiny magnets. The orientation of the spin vector and therefore the orientation of the magnetic moment with respect to a reference axis is quantized and described by the spin quantum number I. For a nuclear spin quantum number I, there are $2I + 1$ possible orientations. The length of the **I** vector is $[I(I + 1)]^{-1/2}\hbar$. The magnetic moment of a nucleus A is proportional to its spin angular momentum $\mathbf{I}_A$ and is given by

$$\mathbf{m}_A = \gamma_A \mathbf{I}_A \qquad (1)$$

The constant of proportionality, γ_A, is called the nuclear magnetogyric ratio. For atomic nuclei it is determined from experiment rather than calculated theoretically.

Electrons also have a spin angular momentum **S** with an electron spin quantum number of $S = ½$. The magnetogyric ratio γ_S for the electron spin magnetic moment $\mathbf{m}_S$ is approximately twice that for the orbital motion, that is, $\gamma_S = g_e\gamma_e$, with $g_e \approx 2.0023$ being the g *factor* of the electron. If an atom or a molecule has all orbital levels doubly occupied there is no net electron spin magnetic moment present (other than the tiny induced magnetic moments due to the presence of magnetic nuclei as will be discussed below). We will restrict the discussion to such systems here.

Interaction of Magnetic Dipole Moments and Magnetic Fields

The interaction energy of a magnetic dipole moment **m** with a magnetic field **B** is given as

$$\Delta E = -\mathbf{m}\cdot\mathbf{B} = -\left(m_x B_x + m_y B_y + m_z B_z\right) \qquad (2)$$

Owing to the negative sign, the energy E is lowest if the orientation of the magnetic field and the magnetic dipole are *parallel*; it is highest if their orientation is antiparallel. This is the mechanism that keeps a compass needle aligned with the Earth's magnetic field.

Since a nuclear spin represents a tiny magnet it will also adopt an orientation relative to a magnetic field in such a way as to minimize its energy. The main difference between a nuclear spin and a compass needle is that the possible orientations of the nuclear magnetic dipole with respect to the magnetic field direction *are quantized.* One of the $2I + 1$ possibilities will correspond to the parallel orientation and thus be lowest in energy; the other orientations have higher energies. Transitions between these energy levels require a specific quantized amount of energy. This forms the basis of nuclear magnetic resonance (NMR).

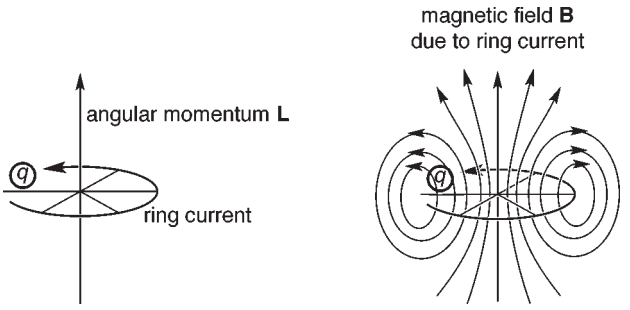

Figure 1. A rotating particle with a charge q has an angular momentum **L**. The charge rotation also represents a ring current that is the source of a magnetic field and a magnetic dipole moment. The magnetic moment **m** is proportional to **L**. The magnetic field is symbolized here by field lines.

Nuclear Spin–Spin Coupling and NMR

Consider two magnetic nuclei A and B in a molecule. Since nucleus A is the source of a magnetic field, the other nucleus B will behave like a "quantum compass needle" in this magnetic field. This results in a set of quantized orientations with quantized energy levels for this nuclear spin. A phenomenological energy expression that describes the energy of interaction between the two nuclei is

$$\Delta E = \mathbf{m}_A\left[\mathbf{K}(A,B) + \mathbf{D}(A,B)\right]\mathbf{m}_B = \sum_{\substack{i=\\x,y,z}}\sum_{\substack{j=\\x,y,z}} m_{A,i}\left[K_{ij}(A,B) + D_{ij}(A,B)\right]m_{B,j} \qquad (3)$$

The two 3 × 3 matrices **K** and **D** relate the interaction of the x, y, z component of one nuclear spin magnetic moment to the x, y, z component of the other nuclear spin magnetic moment. They mediate the strength of the nuclear interaction; for example, they depend on the distance between the two nuclei, the relative orientation of their spins, and in the case of **K** on the details of the molecule's electronic structure. **D** is the *dipolar coupling tensor* and yields the interaction energy between the two nuclei in the absence of electrons (through–space coupling). **K** is called the *reduced indirect spin–spin coupling tensor* that describes the interaction of the nuclei *through their interactions with the electrons of the molecule.* In solution or gas phase where molecules can rotate freely, the dipolar coupling averages to zero *(25)* and only the indirect coupling can be observed easily. Therefore, we will only consider indirect spin–spin coupling here.

Nuclear spin–spin coupling takes place independent of whether there is an external magnetic field present or not. However, it is most conveniently detected via the fine structure of NMR spectra and thus often called "NMR spin–spin coupling". In the NMR experiment one aims to measure transitions between the energy levels of a magnetic nucleus. The splitting of these levels results from applying a strong magnetic field (due to quantized orientations, as outlined above).

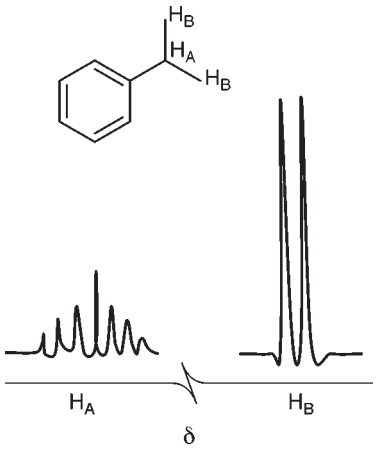

Figure 2. Influence of nuclear spin–spin coupling on the fine structure of the NMR spectrum. Qualitative spectrum for the aliphatic protons of the compound shown. The six methyl protons H_B are equivalent. The proton is an $I = {}^1/_2$ nucleus with two possible orientations with respect to a field direction. The energy levels of the six H_B in the local field are split according to the two possible orientations of the spin of the single H_A, leading to the doublet signal. The energy levels of H_A are split by all possible 2^6 orientations of the six H_B spins. Many of the resulting energy levels have the same energy, leading to a characteristic septet NMR signal with intensity ratios of 1:6:15:20:15:6:1. Intensities and splittings here are not to scale. Coupling with other nuclei in the molecule was not considered. Adapted from ref *26*.

The local magnetic field, $\mathbf{B}^{\text{local}}$, "seen" by a nucleus is not exactly the external field $\mathbf{B}^{\text{ext}}$ generated by the magnet of the NMR spectrometer. The external field is *shielded* by the electrons around the nucleus (nuclear magnetic shielding). We have[2]

$$B^{\text{local}} = (1 - \sigma_A) B^{\text{ext}} \tag{4}$$

where σ_A is the nuclear magnetic shielding constant for nucleus A, which depends sensitively on the chemical environment, B^{local} is the magnitude of the local magnetic field, and B^{ext} is the magnitude of the external field magnetic field. Typically σ_A is quite small, on the order of 10^{-6} to 10^{-3}.

The possible energy levels of the nucleus in the local field depend according to eq 2 on the magnitude of $\mathbf{B}^{\text{local}}$ and $\mathbf{m}_A$. Measuring these energy levels would effectively amount to measuring σ_A if B^{ext} could be measured with high precision. Unfortunately, this is not easy to accomplish. However, the *difference* between the shielding constants of a nucleus in different chemical environments can be measured in NMR experiments very precisely. This quantity is called the *chemical shift* δ_A, where the reference nucleus is usually that of a well-defined standard: $\delta_A = \sigma_{\text{ref}} - \sigma_A$. The energy levels of the probe nucleus are then further split by spin–spin coupling according to eq 3, leading to a fine structure of the NMR spectrum that contains detailed information about the chemical neighborhood of a nucleus. The magnitude of the splitting and the splitting pattern depends on the nuclear spin quantum numbers, the number of nuclei nearby, and the strengths of the spin–spin couplings (Figure 2).

The indirect reduced spin–spin coupling constant K measured in solution or gas phase is the rotational average of the $\mathbf{K}$ tensor and given as $({}^1/_3)(K_{xx} + K_{yy} + K_{zz})$ (isotropic coupling; a similar relationship holds for the isotropic chemical shift). In experimental work, "J coupling constants" are reported because it is more convenient to extract J coupling constants directly from the line splittings in the NMR spectrum. They are related to the K coupling constant by a simple pre-factor that includes both nuclear magnetogyric ratios and Planck's constant:

$$J(\text{A,B}) = \frac{h}{4\pi^2} \gamma_A \gamma_B K(\text{A,B}) \tag{5}$$

The K couplings are given in SI units of $T^2\ J^{-1}$ or $kg\ m^{-2}\ A^{-2}\ s^{-2}$, with typical magnitudes between 10^{18} to 10^{22}. We will from now on only refer to J couplings, which are given in hertz (s^{-1}), with typical magnitudes of 10^{-1} to 10^3.

Mechanisms for J Coupling

J coupling is the interaction between two magnetic nuclei mediated by the electrons in a molecule. There are two basic mechanisms. The magnetic field of a nucleus locally induces a magnetic moment in the electronic system. This electronic magnetic moment can occur in form of either (i) an electron spin polarization, that is, a local increase or decrease of the probability of finding spin-up (alpha) versus spin-down (beta) electrons[3] or (ii) by inducing orbital ring currents (Figure 3). The motion of electrons in a many-electron system is coupled by their electrostatic Coulomb interaction. Thus, local effects such as the locally induced electronic magnetic moment will have an effect on the electronic structure elsewhere in a molecule. The locally induced magnetic moment is transferred to other parts of the molecule, mainly through the chemical bonds. It is then "detected" by another nucleus, that is, the transferred-induced electronic magnetic moment interacts with the local magnetic field of the other nucleus according to eq 2. Generally, a pronounced distance effect can be observed. The more bonds there are in between the two nuclei, or the larger the internuclear distance, the weaker the J coupling. A typical sign pattern might also be observed, as discussed briefly later for two- and three-bond couplings.

Both the spin and the orbital mechanisms are, for theoretical reasons, usually further subdivided. In Appendix A in the Supplemental Material,[W] we outline briefly how the five different coupling mechanisms are obtained in a quantum mechanical treatment of a molecule. For short-range coupling through one or a few bonds, *usually* the Fermi contact (FC) mechanism is the dominant one. It is part of the spin mechanism shown in Figure 3. The FC mechanism originates in a spin polarization of the electronic system *right at* one of the nuclei, and the resulting interaction of the transferred spin polarization *right at* another nucleus. In computations, atomic nuclei are usually treated as point charges and point magnetic

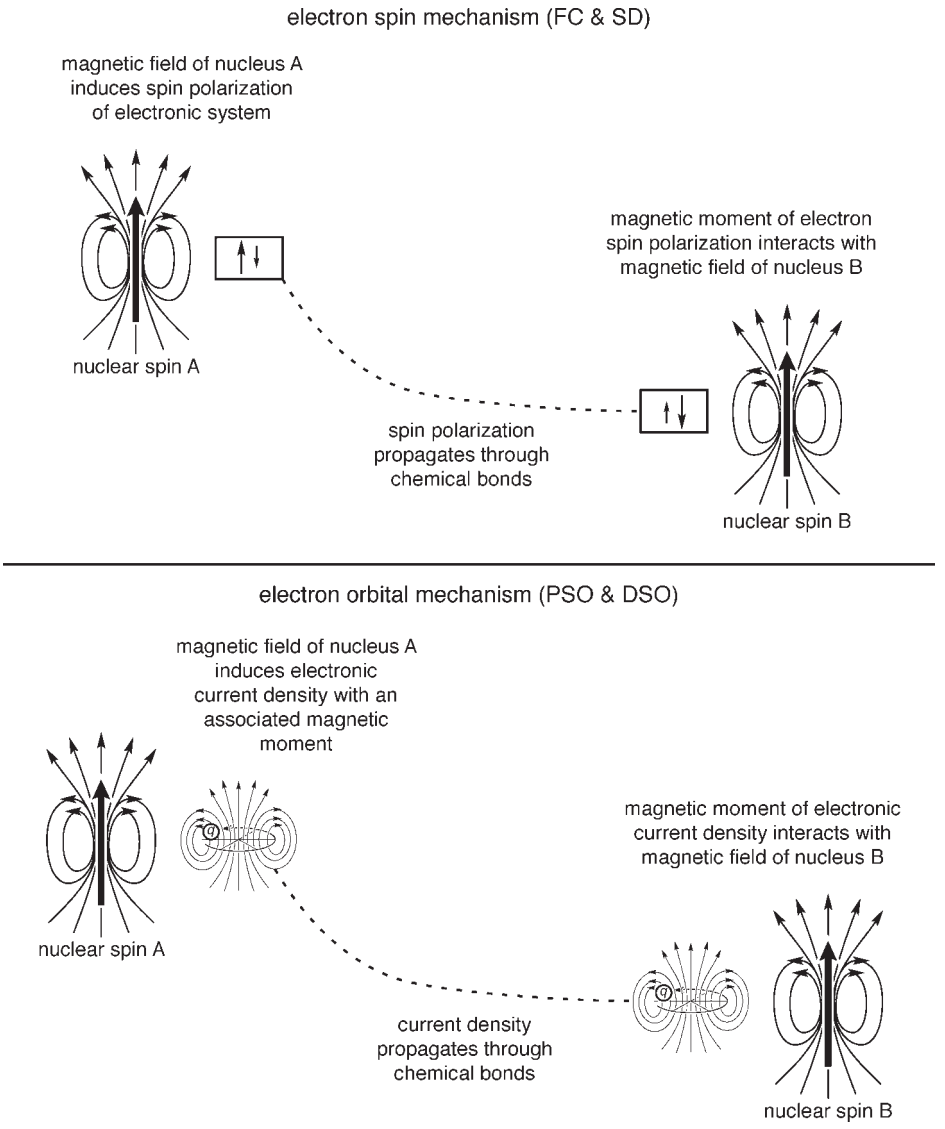

Figure 3. Mechanisms of indirect nuclear spin–spin coupling: (Top) The magnetic field of the nucleus (indicated by field lines) induces a spin polarization in the electronic system that is transferred through the chemical bonds to another nucleus. This spin polarization carries its own magnetic moment that interacts with the magnetic field of the other nucleus. (Bottom) Instead of inducing a magnetic moment in the electronic system via the electron spin, the nucleus induces orbital currents with an associated magnetic moment that get transferred through the chemical bonds to another nucleus.

dipoles. The "contact" term is then caused by the interaction of the nuclear with the electron spin at the locations of the point nuclei. The remainder of the electron spin mechanism is labeled "spin–dipole" (SD). It samples electronic positions other than the exact locations of the nuclei but is usually negligible except, typically, for triple-bonded pairs of nuclei *(3)* and for long-range couplings. Further, there is a FC–SD cross term, that is, the FC mechanism on the one nucleus is "detected" by the SD mechanism on the other nucleus and vice versa. It turns out that this mechanism only contributes to the **J** tensor but averages to zero for the resulting *J* coupling constant.

The orbital current mechanism is divided into a "paramagnetic" and a "diamagnetic" part (PSO for "paramagnetic" and DSO for "diamagnetic spin–orbital" mechanism). They can be distinguished in the theoretical formalism in the way they appear in clearly separated terms. However, only their sum is physically meaningful. Typically, the PSO mechanism yields a negative contribution to the coupling, which is often small. It can be large for p-bonded systems such as interhalogen diatomics *(27)*. The DSO mechanism is usually negligible. An important exception are the H−H coupling constants in H_2O and its heavier chalcogen analogs *(3)*.

It needs to be highlighted that experimentally only the sum of all mechanisms is observable. Whether the *J* coupling constant is positive or negative depends on the relative weight of the mechanisms, their sign, and the signs of the nuclear magnetogyric ratios γ_A, γ_B.

Molecular Orbital Methods

To further discuss theoretical details we introduce an expression for *J* coupling within a *molecular orbital* (MO) approach. This can be the Hartree–Fock, or DFT, or semi-empirical methods. To derive the expression the recipe given in the Appendix (see the Supplemental Material[W]) can be followed. There, we used a sum over the excited state wavefunctions to describe the perturbation of the ground-state wavefunction. Here, a sum over vacant MOs is needed for *each* occupied MO φ_i instead. We will call this "mixing of vacant with occupied orbitals". The sum over vacant orbitals describes the spin polarization and orbital currents induced by the presence of the nuclear spins. For the reason of this "mixing" see below. An element of the reduced coupling tensor is

$$K_{x,y}(\mathrm{A},\mathrm{B}) = 2\mathrm{Re}\sum_{i}^{\mathrm{occ}}\sum_{a}^{\mathrm{vac}}\frac{\left\langle\varphi_i \left| \hat{h}_x^{(\mathbf{m}_\mathrm{A})} \right| \varphi_a\right\rangle\left\langle\varphi_a \left| \hat{h}_y^{(\mathbf{m}_\mathrm{B})} \right| \varphi_i\right\rangle}{\varepsilon_i - \varepsilon_a} + \sum_{i}^{\mathrm{occ}}\left\langle\varphi_i \left| \hat{h}_{x,y}^{(\mathbf{m}_\mathrm{A},\mathbf{m}_\mathrm{B})} \right| \varphi_i\right\rangle \quad (6)$$

where Re means the real part is to be taken. The *J* coupling is obtained from $(1/3)(K_{xx} + K_{yy} + K_{zz})$ by applying the conversion factor of eq 5. The φ's are the occupied and vacant MOs, the ε's their energies, and the $\hat{h}$'s are the Cartesian components of the $\mathbf{m}_\mathrm{A}$ and $\mathbf{m}_\mathrm{B}$ derivatives of the operators listed in the Appendix, eqs 28 to 31 (see the Supplemental Material[W]). The operator $\hat{h}^{(\mathbf{m}_\mathrm{B})}$ is a sum of the Fermi contact (FC), the paramagnetic (PSO), and the spin–dipole (SD) term for nucleus A. We can write $\hat{h}^{(\mathbf{m}_\mathrm{A})} = \hat{h}_\mathrm{A}^{\mathrm{FC}} + \hat{h}_\mathrm{A}^{\mathrm{PSO}} + \hat{h}_\mathrm{A}^{\mathrm{SD}}$. The operator $\hat{h}^{(\mathbf{m}_\mathrm{B})}$ contains the equivalent operators for nucleus B. The operator $\hat{h}^{(\mathbf{m}_\mathrm{A},\mathbf{m}_\mathrm{B})}$ is responsible for the diamagnetic orbital mechanism (DSO). Either $\hat{h}^{(\mathbf{m}_\mathrm{A})}$ or $\hat{h}^{(\mathbf{m}_\mathrm{B})}$ must also include an additional term that describes the perturbation of the molecule's Coulomb and exchange potential *(23)*. For illustrative aspects this term can be neglected, though it must be present in the actual computations. This term is the reason why an iterative self-consistent field (SCF) cycle is performed by programs that calculate *J* coupling.

Why Vacant Orbitals or Excited States?

It is perhaps at first sight not so intuitive why the MO equation for *J* coupling needs to involve vacant orbitals.[4] Initially, the occupied orbitals are obtained without considering the presence of nuclear spins. Each orbital is doubly occupied, therefore there is no spin polarization present. Likewise, there is no total orbital current. To describe the spin polarization and orbital currents induced by the nuclear spins (see Figure 3) one needs to add ("mix") other functions into the set of occupied orbitals to describe these "deformations". Using the vacant orbitals is one way of achieving this. This is a more mathematically motivated explanation. Alternatively, one can think of a fraction of the vacant orbitals with alpha or beta spin (spin polarization), or with an orbital angular momentum (orbital ring currents), to become partially populated under the influence of the nuclear spin's magnetic field.[5] The numerator in eq 6 to some extent defines how strongly the presence of the nuclear spins "mixes" higher lying orbitals into the ground state. This provides a measure of how good a particular vacant orbital is suited to describe the spin polarization and current densities. The higher its energy the more the vacant orbital differs from the occupied orbitals. In the alternative explanation scheme, the higher lying the vacant orbital is, the less likely it is to become partially occupied. The occurrence of the energy denominators in eq 6 can be qualitatively understood as a weighting scheme such that the small influence from the nuclear spins deforms the ground-state electronic structure as little as possible, but as much as necessary.

Atomic Orbital Contributions to J Coupling

Equation 6 underlies qualitative theoretical interpretations of *J* couplings. For example, consider the Fermi contact (FC) mechanism. Let $\hat{h}_\mathrm{A}^{\mathrm{FC}} = (4\mu_0\beta\hbar/3)\hat{S}_z\delta(\mathbf{r}_\mathrm{A})$ be the Fermi contact operator for nucleus A. Here β is Bohr magneton, $\hat{S}_z$ is the *z* component of the electron spin operator, δ is the Dirac delta function centered on nucleus A, and μ_0 is the permeability of free space. In atomic units as used in the appendix, the prefix reads $(8\pi/3c^2)$. Similarly, $\hat{h}_\mathrm{B}^{\mathrm{FC}} = (4\mu_0\beta\hbar/3)\hat{S}_z\delta(\mathbf{r}_\mathrm{B})$ is the FC operator for nucleus *B*. The operators are obtained by differentiating the first term in eq 29 of the Appendix (see the Supplemental Material[W]) with respect to the *z* component of $\mathbf{m}_\mathrm{A}$ and $\mathbf{m}_\mathrm{B}$, respectively. We chose the *z* component for convenience. The FC term is isotropic, that is, $K_{xx} = K_{yy} = K_{zz}$. The MO expression, eq 6, contains the product of $\langle\varphi_i|\hat{h}_\mathrm{A}^{\mathrm{FC}}|\varphi_a\rangle$ and $\langle\varphi_a|\hat{h}_\mathrm{B}^{\mathrm{FC}}|\varphi_i\rangle$ integrals. These integrals sample the value of the product $\varphi_i\varphi_a$ at nucleus A and B, respectively, because of the delta functions in the operators (this is where the label "contact" stems from). Recall that $\int dx \cdot f(x)\,\delta(x - a) = f(a)$. Thus, we have

$$\left\langle\varphi_i\left|\hat{h}_\mathrm{A}^{\mathrm{FC}}\right|\varphi_a\right\rangle = \mathrm{const}\cdot\varphi_i(\mathrm{nucleus\ A})\cdot\varphi_a(\mathrm{nucleus\ A}) \quad (7)$$

and an equivalent expression for $\langle\varphi_i|\hat{h}_\mathrm{A}^{\mathrm{FC}}|\varphi_a\rangle$. Because

$$\hat{S}_z = \frac{\hbar}{2}\begin{bmatrix}1 & 0\\ 0 & -1\end{bmatrix}$$

the FC operator acts with opposite sign on spin-up (alpha) and spin-down (beta) orbitals, which is how this mechanism causes a spin–polarization. The LCAO–MO approximation (linear combination of atomic orbitals) is convenient to interpret eq 7 further. In the LCAO approach, each MO is represented as a linear combination of atomic orbitals (AOs), that is,[6]

$$\varphi_i = \sum_{\mu}^{\mathrm{basis}}\chi_\mu C_{\mu i} \quad \text{example:} \quad \varphi_i = \text{(A)(B)} \quad \text{or} \quad \varphi_i = \text{(A)(B)} \quad (8)$$

The $C_{\mu i}$ are the MO coefficients. Equation 8 also displays examples for symbolic versions that are more familiar to students, using graphical symbols for each AO χ_μ. We recall that only s AOs have a nonzero value at the nucleus where they are centered. From this and eq 7, it becomes clear that

only MOs with a significant s character on ***both*** *atoms A and B can contribute significantly to the FC mechanism*. These are the orbitals of (local) σ character. It is not vital to use the equations to make this point if the students accept the following without proof: (i) The spin mechanism for *J* coupling contains a contact term. It samples the value of the induced spin polarization that is described by products of occupied with vacant orbitals, *at both* nuclei simultaneously. (ii) Only molecular orbitals with s character on both centers A and B will have a nonzero value at both nuclei.

From an analysis of the other operators (PSO, SD) one can deduce in a similar fashion that orbitals with either p_σ or p_π character contribute to the paramagnetic orbital (PSO) term, that orbitals with p_π character contribute to the spin–dipole (SD) term, and so forth *(13).* However, an estimate of the various contributions in eq 6 without actually calculating anything can only be made in very simple, clear-cut, usually highly symmetric cases. Even then, for a student who is trying to get some idea of the theoretical background of NMR the situation might not be obvious at all. Thus, we see a great benefit in actually *first computing and then analyzing orbital contributions* to *J* coupling even for simple molecules. This way, by linking the results to graphical representations of the orbitals, the approach can be made visual and numerically accurate at the same time. The MO foundation of Kohn–Sham DFT makes it ideal for such analyses.

The s Character and the FC Mechanism

From the analysis presented in the previous section one may conclude that *J* couplings should strongly depend on the amount of s character in the hybrid atomic orbitals that form the bonds between the two coupled nuclei (e.g., sp, sp^2, sp^3). For one-bond C−C and C−H couplings this is indeed often found experimentally and backed up by theoretical data. We will return to this topic in more detail later since it is an ideal target for a computational course assignment. One problem with the hybridization argument is that it reflects only the electronic structure of the ground state. As already mentioned, the FC mechanism induces a spin density in a molecule. The magnitude of the spin density is not only determined by the s character of the bonds in the ground state. The hybridization in the excited states determines the ease by which such a spin density can be induced in the molecule by one nucleus and how effectively it is transferred to another one. Systems with comparable s character in their bonds and comparable bond strengths, in particular in transition-metal chemistry, can afford orders of magnitude different coupling constants because of low-lying vacant orbitals with high s-antibonding character *(22).* A detailed analysis of a calculation can expose such situations.

The Energy Gap

Without considering the magnitude of the numerator in eq 6, the FC mechanism will be rather large if the molecule has high-lying σ-type and low-lying σ*-type orbitals because $(\varepsilon_i - \varepsilon_a)^{-1}$ will be large. Sometimes, just by considering the energy gap for closely related systems one can rationalize trends for coupling constants. The HOMO–LUMO gap itself, on the other hand, is not always the correct measure since both HOMO and LUMO might not contribute to the coupling because they yield small to vanishing numerators in eq 6. An example would be a coupling constant that is dominated by the Fermi contact mechanism in a system with frontier orbitals of π character.

Canonical and Localized MOs

One important aspect about MOs is that they are not unique. The orbitals in eq 6 are the so-called *canonical* orbitals, which are the most convenient to obtain in a computation. These orbitals are mutually orthogonal *and delocalized* by construction. Therefore, they are useful for describing global phenomena such as ionization, excitations, and so forth. *Localized* orthogonal MOs λ_p (LMOs) can be constructed from the canonical orbitals φ_i by a linear combination of the φ_i with coefficients U_{ip} to yield $\lambda_p = \Sigma_i \varphi_i U_{ip}$. In the Boys procedure *(28, 29),* the *U* coefficients are determined computationally based on a criterion that minimizes the spatial extent of the LMOs and preserves the orthonormality of the orbitals. In effect, LMOs are the mathematical equivalent of bonds, lone pairs, and core orbitals in a molecule. Because they are spatially localized they are well-suited to interpret local phenomena such as local reactions or NMR parameters. A set of canonical MOs yields the same electron density as a set of LMOs. The basic theorem of DFT states that the density defines all other molecular properties. Thus, there is really no way to select one or another set of orbitals as more meaningful.

Various Decomposition Methods

Later, we will make use of a number of numerical decomposition schemes for *J* couplings. We will focus on the FC contribution $J^{FC}(A,B)$ to the coupling for two reasons: (i) The coupling in the examples discussed later is strongly dominated by the FC mechanism and (ii) the FC mechanism is isotropic ($J_{xx} = J_{yy} = J_{zz}$) and therefore easier to analyze than the three principal components of the PSO, DSO, and SD mechanisms. For explicit expressions of the decompositions we used we refer the reader to ref *22.*

The MO Decomposition

This decomposition scheme derives directly from the double sum in eq 6 and yields contributions to the Fermi contact part $J^{FC}(A,B)$ from each occupied–vacant $(\varphi_i–\varphi_a)$ orbital pair after conversion from *K* to *J* coupling units:

$$J^{FC}(A,B) = \sum_{i}^{occ}\sum_{a}^{vac} J_{ai}^{FC}(A,B) \qquad (9)$$

Thus, a list of occ–vac (*ai*) contributions to the *J* coupling identifies pairs of σ and σ* orbitals that are mainly responsible for the FC mechanism. To obtain a single contribution to the *J* coupling from each occupied MO, we simply sum over all vacant orbital contributions:

$$J^{FC}(A,B) = \sum_{i}^{occ} J_i{}^{FC}(A,B) \qquad (10)$$

where $J_i^{FC}(A, B) = \Sigma_a^{vac} J_{ai}{}^{FC}(A,B)$. Thus, the J_i^{FC} include the effects of spin polarization of the occupied orbital φ_i. An advantage is that the MO decomposition leads to the most

straightforward analysis scheme but as we will see later, the results are not always the most intuitive.

The FO and LMO Decompositions

The coupling constant can alternatively be expressed as

$$J^{FC}(A,B) = \sum_p \sum_q J_{pq}^{FC}(A,B) = \sum_p J_p^{FC}(A,B) \quad (11)$$

where p and q now refer to a pair of localized MOs (LMOs) or fragment orbitals (FOs), respectively. Again, we can define $J_p^{FC} = \Sigma_q J_{pq}^{FC}$ to reduce the amount of detail in the analysis. For most LMOs, the main contributions in this decomposition scheme arise from single "diagonal" terms (i.e., $J_p^{FC} \approx J_{pp}^{FC}$). Further, for LMOs the summations in eq 11 only involve *occupied* orbitals. The spin–polarization contributions from unoccupied orbitals are already absorbed in each term. Equation 11 for LMOs is therefore the equivalent of eq 10, not eq 9. For the FO analysis, both occupied and unoccupied fragment orbitals can enter eq 11.

We will show in the following section with some well-studied examples how such decompositions can give some pictorial insight into C−C coupling constants. It needs to be emphasized that these and other possible decompositions can be chosen almost arbitrarily since they must all yield the same final result. However, one of them might be of particular advantage for developing an understanding of *J* coupling.

Calculation of *J* Couplings for Ethane, Ethene, Ethyne, and Benzene

Practical Aspects; Use of the Material

There are a number of different *J* coupling terms (FC, SD, PSO, DSO) that arise from its theoretical treatment. Further, the whole tensor needs to be calculated to obtain the coupling constant as its rotational average. This can make *J*-coupling computations confusing for students. However, we believe that the qualitative part of the previous section provides sufficiently detailed reasons why there are several different terms that have to be calculated and what the underlying physical mechanisms are.

DFT calculations of *J*-coupling constants are quite straightforward otherwise. Apart from choosing a suitable basis set and functional, most programs can be used as a "black box" if necessary. For instructional purposes, triple-ζ polarized standard basis sets such as the 6-311G** or TZVP Gaussian-type basis sets or a Slater-type basis of equivalent flexibility should yield sufficient accuracy to obtain correct signs and orders of magnitudes for *J*-coupling constants. Suitable choices for density functionals in *J*-coupling calculations are, for example, the hybrid functionals B3LYP or PBE0 and the gradient corrected nonhybrid functionals BP86 or PBE. Commercially available quantum chemistry programs that can calculate NMR properties at the DFT level in a "black box" manner are, for example, Gaussian '03 *(30)* and ADF *(31)*. We have used ADF for this project. An instructor might prefer to use a different quantum chemistry code to calculate *J* couplings where some of the analysis features might not be available. In this case we suggest to use our calculated results as an illustration of how an orbital-based numerical analysis can be applied to analyze *J* coupling. The qualitative features of the MO and LMO graphics as well as the magnitude of the calculated coupling constants will be similar enough between different DFT packages to obtain the same conclusions. For some software packages including Gaussian, the NBO program provides analysis tools for NMR parameters *(32)*.

On the theoretical side, it is relatively straightforward to derive a general sum-over-states (SOS) expression for spin–spin coupling in a course as long as the students can understand eq 17 of the Appendix (see the Supplemental Material[W]). The derivation can be accomplished within a two-hour lecture. We think it is beneficial to discuss the statement often found in research articles that "the perturbation mixes excited states into the ground state". The detailed form of the operators is more difficult to derive in class since it requires a fair quantity of vector calculus. We do not regard this as an essential step for a more practically oriented computational chemistry course or as part of an NMR course or an NMR section of an organic chemistry course. However, the instructor might want to outline how these operators are obtained. For a more theoretically oriented class, the derivation of some of the simpler operators could then be left as an exercise. We have included in the Appendix a brief outline of how the operators for spin–spin coupling are obtained (see the Supplemental Material[W]). On the practical side, preliminary work that covers a range of typical computational chemistry tasks might be carried out by the students before actually analyzing *J* couplings. This may include optimization of the molecule's geometries, a calibration study of calculated *J* couplings using various density functionals or basis sets, or a brief bibliographic search to find the necessary experimental data.

The computation of the C−C and C−H *J* couplings in a set of 4 hydrocarbons (ethane, ethene, ethyne, and benzene) was initially assigned to a second-year undergraduate chemistry major during the second half of a 1 credit (3 hrs/week for 15 weeks) project. The student had some basic knowledge of NMR from an organic chemistry class but no prior experience with computational chemistry. His work provided us with the calculated values of the C–C coupling constants, the data for the analysis in MO, LMO, and FO contributions, and some of the orbital graphics. The student quickly acquired the knowledge of how to do the calculations after being told that the DFT program is able to calculate molecular orbitals. We did not make an attempt to introduce him to theoretical aspects beyond what is presented at the beginning of the previous section but rather let him focus on the intuitive graphical aspects of the work (i.e., on-screen graphics of molecular structures, plots of molecular orbitals) and the *J*-coupling calculation in a black-box fashion. The analysis of the raw data was later carried out by us. Initially, the student was asked to perform a DFT calibration study to determine which basis set and functional would yield reasonable agreement with experimental data. Basis sets were described to him as "poor", "good", "better", and so forth without further detail.

Subsequently, we have used the material as part of a three-credit hour special topics course on molecular properties that was attended by four chemistry graduate students and one fourth-year undergraduate chemical engineering major. The theory outlined in the Appendix (see the Supplemental Material[W]) was presented in detail (including NMR shifts, polarizabilities, and other properties) during the lectures over the course of five weeks. One week was devoted to refreshing the basic theorems of quantum theory, and one week to in-

structions on how to use a Linux system and run quantum chemistry software. Some of the operators were derived in class to demonstrate the method by which they are obtained. The full list of NMR-relevant operators was then provided as a handout along with some key formulas such as the SOS equation. One of the assignments in the five-weeks unit was to perform calculations of NMR chemical shifts and spin–spin coupling constants for ethane, ethene, ethyne, and in particular to study the dependence of the C−C and C−H coupling constants on the carbon hybridization. The analysis described here was presented and discussed in class to clarify the origin of the *J* couplings and the connection with the carbon hybridization. (With a larger class, we envision one group calculating the *J* couplings while another group generates the orbital plots, later to be analyzed and discussed jointly.) Provided with step-by-step instructions on how to run the software on a Linux system, none of the students reported problems regarding the computational part. For the computations the class was given accounts on one of our group's Linux PCs (PIV, 2.4 GHz, 512 MB). The available graphical user interface (GUI) was not employed because of the simple structure of the molecules. Instead, we have provided our students with a link to the CCCBDB Web site *(33)* where they were able to obtain experimental geometries for direct use in the calculations. Owing to the low computational cost (on the order of a few minutes per coupling constant) we had no problems regarding simultaneous use of the single-processor machine. In the five-week NMR unit of our graduate course, the focus was on the formalism. Our students experienced the calculations as a great help to make sense of the theoretical formalism and the explanations given in class.

Computational Details

Density functional (DFT) computations were carried out with the Amsterdam Density Functional (ADF) program package *(34–38)*. We have used a Linux version but the program is available for Windows and Mac OS-X as well. To generate localized orbitals, the input key **LOCORB STORE / END** was applied in the ADF calculations. *J* couplings were performed with ADF's "CPL" module *(36–38)*. The coupling constant analysis was enabled by using the **CONTRIBUTIONS** subkey in the CPL input with the option LMO or SFO *(36)*. Orbital plots were prepared with MOLEKEL *(39)* and an orbital plotting tool for ADF available free of charge from our Web site *(40)*. Alternative no-cost graphical tools that could be used for this purpose are, for example, MOLDEN *(41)* or GOPENMOL *(42)*, which also work well with other quantum chemistry codes. For an input example and a guide through the output please see the Supplemental Material.[W]

Computations for the main bond distances and *J*-coupling constants were performed with the Becke and Perdew (BP86) *(43, 44)* GGA functional and the triple-ζ polarized (TZP) all-electron Slater-type basis. The carbon 1s shell was kept frozen in the geometry optimizations. Very similar *J* couplings would be obtained with experimental geometries. It is possible to obtain somewhat better agreement with experiment by using hybrid functionals that are, however, not available with the software we used. For the intended instructional purpose the accuracy that is achieved with a GGA functional is certainly sufficient while the computational effort is particularly low. Differences between computations and experiment mainly arise from neglected electron correlation effects, DFT self-interaction errors, incomplete basis sets (more polarization functions and high-exponent 1s functions would be needed), and zero-point vibrational averaging. *J* couplings are sensitive and therefore not easy to calculate with very high accuracy.

Table 1. Selected Experimental and Calculated Bond Lengths *d* in Å, and One-Bond Spin–Spin Coupling Constants *J* in Hz[a,b]

Variable	Molecule (Symmetry)			
	C_2H_2 (C_{2h})	C_2H_4 (D_{2h})	C_2H_6 (D_{3d})	C_6H_6 (D_{6h})
d(C–C)	1.207 (1.203)	1.335 (1.339)	1.532 (1.536)	1.399 (1.397)
d(C–H)	1.071 (1.063)	1.092 (1.086)	1.100 (1.091)	1.092 (1.084)
J(C,C)	208.6 (172.7)	73.4 (67.8)	29.3 (34.5)	57.9 (56.2)
J^{FC}(C,C)[c]	202.5	82.7	29.3	64.2
J(C,H)	272.7 (248.2)	164.4 (156.2)	136.3 (124.4)	166.2 (157.7)
J^{FC}(C,H)[c]	272.7	163.3	134.4	165.0

[a]BP86 functional, TZP basis. [b]The experimental bond lengths and *J* couplings, in parentheses, are from refs *33* and *13*, respectively. [c]Calculated Fermi–contact term only.

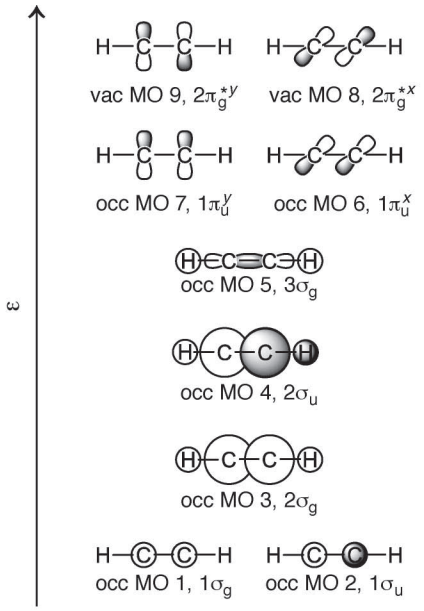

Figure 4. The occupied and vacant MOs of ethyne written in the pictorial form of eq 8. For plots of these MOs, see Figure 5. The energy axis is not to scale.

Ethyne: Geometries and Coupling Constants

Our results are listed in Table 1. As expected, the FC mechanism yields the main contribution to the *J* couplings in our set of small hydrocarbons. The analysis will thus focus on this term. Some comments on the SD and PSO terms will be given near the end of the article. We start with the ethyne molecule to introduce the different analysis concepts outlined in the theoretical section.

Ethyne: MO Analysis of *J*(C,C)

The canonical MO-based analysis is obviously most closely related to the (canonical) MO diagram of the molecule, which is depicted qualitatively in Figure 4. The total

Table 2. Canonical MO Contributions to $^1J^{FC}$(C,C) in Ethyne, in Hz[a]

Occ MO	Vac MO[b]					Total[c]
	29	47	48	49	50	
1	1678.0	-2096.5	1693.7	-32818.4	33052.7	1311.4
2	-1682.5	2096.4	-1696.9	32854.7	-33085.4	-1318.2
3	531.5	-254.5	180.5	-2090.2	2080.9	425.1
4	-249.4	112.9	-80.8	914.0	-909.9	-215.7
sum	277.6	-141.7	96.5	-1139.9	1138.3	202.5

[a]BP86 functional, TZP basis. [b]Occ MO and Vac MO are the φ_i and φ_a in eq 9, respectively. [c]Total includes contributions from all vacant orbitals and represents eq 10.

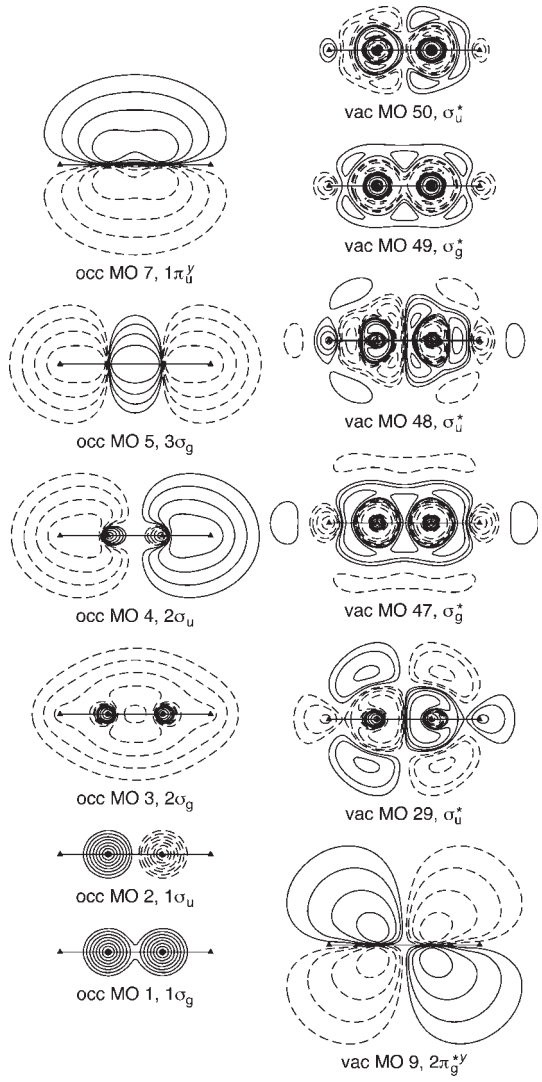

Figure 5. Some MOs of ethyne. The MOs are plotted in the *y*–*z* plane with *z* along the C−C bond. The contour values are ±0.02 × 2^n, n = 0, 1, 2,... $(e/a_0^3)^{1/2}$; dashed lines indicate negative values. The MOs 6 and 8 ($1\pi_u^x$ and $2\pi_g^{*x}$) are not plotted. They are symmetry–equivalent to MOs 7 and 9, respectively, but lie in the *x*–*z* plane instead.

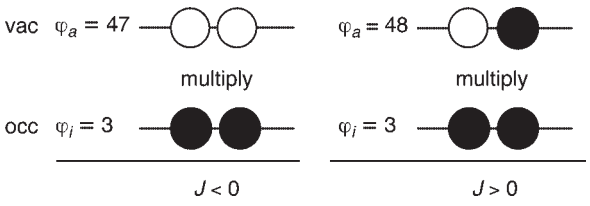

Figure 6. Pictorial representation of eq 12 for the contributions of the "mixing" of occupied σ MO 3 with vacant σ* MOs 47 and 48 to J(C,C) of ethyne. Black (white) circles indicate positive (negative) s-AO coefficients in the MOs. The left sign pattern always leads to a negative FC term, the right one to a positive FC term.

number of MOs (occupied and vacant) is equal to the number of basis functions. In the case of ethyne, the TZP basis in the ADF calculation yields 50 molecular orbitals, 7 of which are doubly occupied. The occupied MOs as well as a number of vacant MOs that contribute strongly to J^{FC}(C,C) are shown in Figure 5. Because of the linear symmetry of ethyne is it beneficial to use 2D contour diagrams. This way, we obtain a more detailed picture of the orbitals than from 3D isosurfaces. We will use 3D isosurface plots where it is important to show the spatial arrangement of orbitals, and later for ethane.

The MO contributions to J^{FC}(C,C) according to eqs 9 and 10 are collected in Table 2. The π orbitals 6 and 7 do not contribute because they have zero s character. Further, MO 5 ($3\sigma_g$, involving carbon p_σ atomic orbitals) has a node on each carbon nucleus and therefore also does not yield any contribution to J^{FC}(C,C). First, we notice two huge core MO contributions (from $1\sigma_g$ and $1\sigma_u$) that cancel almost completely. Thus, despite the huge individual contributions the J coupling is not really caused by these core orbitals but rather by the valence orbitals. This might sound paradoxical because the Fermi contact operators sample the MOs at the nuclei. However, valence MOs must be orthogonal to the core MOs, hence they have core orthogonalization tails that probe the near-nuclear region. In this sense, J coupling should be considered "chemical", that is, a valence shell property despite the fact that the Fermi-contact mechanism probes the orbitals *at* the nuclei.

The mixing of the occupied σ MOs 3 and 4 with high-lying vacant σ-type orbitals 29, 47–50 yields the main contributions to the C–C coupling. The dominant role of these σ MOs in the FC mechanism is expected, because these MOs have a significant s character on both carbon atoms. Let us consider as an approximation just one σ–σ* orbital pair represented by one s orbital on each carbon atom. We use $\varphi_\sigma = C_\sigma(\mathrm{A})s(\mathrm{A}) + C_\sigma(\mathrm{B})s(\mathrm{B})$ and similarly for φ_{σ^*}, where the C's are the LCAO coefficients for the s orbitals as in eq 8. We substitute this in eq 7 and make the approximation that the value of each s orbital at the *other* nucleus is negligible. This yields, from eq 6,

$$J_{\sigma\sigma^*}^{\mathrm{FC}}(\mathrm{A,B}) \approx \mathrm{const}\cdot\frac{C_\sigma(\mathrm{A})C_{\sigma^*}(\mathrm{A})\cdot C_\sigma(\mathrm{B})C_{\sigma^*}(\mathrm{B})}{\varepsilon_\sigma - \varepsilon_{\sigma^*}} \quad (12)$$

with a positive prefactor. For the lower-lying σ orbital we might find that $C_\sigma(\mathrm{A}) = C_\sigma(\mathrm{B})$. For the σ* we expect to have

an additional node and therefore $C_{\sigma^*}(A) = -C_{\sigma^*}(B)$. The orbital denominator in eq 12 is negative. Thus, such a sign pattern yields a positive FC contribution. In case of a larger basis set we have many contributions of the type in eq 12. Some of the vacant MOs can also have like signs on both carbons that would lead to positive numerator and an overall negative FC contribution. The difference of sign observed for the occ–vac contributions is easily explained by the pictorial representation of eq 12 shown in Figure 6, which can also be applied to unsymmetrical molecules. Consider the coupling contributions of orbital 3 ($2\sigma_g$) with MOs 47 and 48 as an example for the relation between the sign patterns and the sign of the coupling contributions. Figure 6 also illustrates why the contributions from MOs 3 and 4 have always opposite sign.

The vacant MOs 47–50 are composed of "pseudo-3s"-type carbon AOs. That is, these AOs have the same number of radial nodes as 3s but are constructed from basis functions that are spatially in the 1s and 2s range (because these are the basis functions we provide in the calculation). It should be noted that the *sum* of the *J* contributions from MOs 49 and 50 is small in all cases. This pair of orbitals is simply enforced by symmetry just as the $1\sigma_g - 1\sigma_u$ pair, but is not of high importance for the coupling.

In summary, we see that the C–C coupling is described by two large contributions from the s–σ bonding MOs 3 and 4 ($2\sigma_g$ and $2\sigma_u$) with opposite signs. The different signs result from the different bonding–antibonding patterns of these orbitals around the carbons.

Ethyne: LMO Analysis of *J*(C,C)

In the last paragraph we have seen that using canonical delocalized MOs to analyze *J* coupling yields a number of huge symmetry-enforced nonintuitive contributions from orbitals that are effectively not involved in the coupling process. Also, the coupling must be finally interpreted in terms of two large terms of opposite sign from occupied bonding and antibonding σ orbitals. Localized MOs (LMOs) are the theoretical representation of bonds, lone pairs, and core orbitals. Thus, a LMO based analysis of *J* coupling might yield smaller contributions that correspond more to chemical intuition.

The seven orthogonal LMOs constructed from the seven occupied MOs by the Boys procedure *(28, 29)* are plotted in Figures 7 and 8. Please note that the numbering of the LMOs as printed in the ADF output does in general not correlate with their energetic ordering. LMOs 1 and 2 are the core 1s orbitals centered on each carbon atom. They are essentially linear combinations of MOs 1 and 2 in the form $(1\sigma_g \pm 1\sigma_u)/\sqrt{2}$. LMOs 4 and 5 represent the two C−H bonds, whereas LMOs 3, 6, and 7 represent the C−C triple bond in form of three equivalent "banana-bond" orbitals with the same LMO energy. Their contributions to the *J* coupling according to eq 11 are listed in Table 3. The LMO contributions are significantly smaller than those from the canonical MOs and also intuitively more predictable. For instance, the largest positive contributions are from the three C−C "banana bonds" (LMOs 3, 6, and 7). The 3 contributions are equal because LMOs 3, 6, and 7 are equivalent. Somewhat less intuitive are the contributions from the carbon 1s orbitals. However, we recall that the LMOs are still mutually orthogonal. This requires the participation of all LMOs in the *J* coupling, including all core orbitals (LMOs 1 and 2). Further, we observe negative contributions to J^{FC}(C,C) from the two C−H bonds (LMOs 4 and 5). An explanation for the sign of these contributions is that the carbon atoms have to provide some share of their electrons to the C−H bonds, which are therefore not available for the C−C coupling. The slight difference observed between

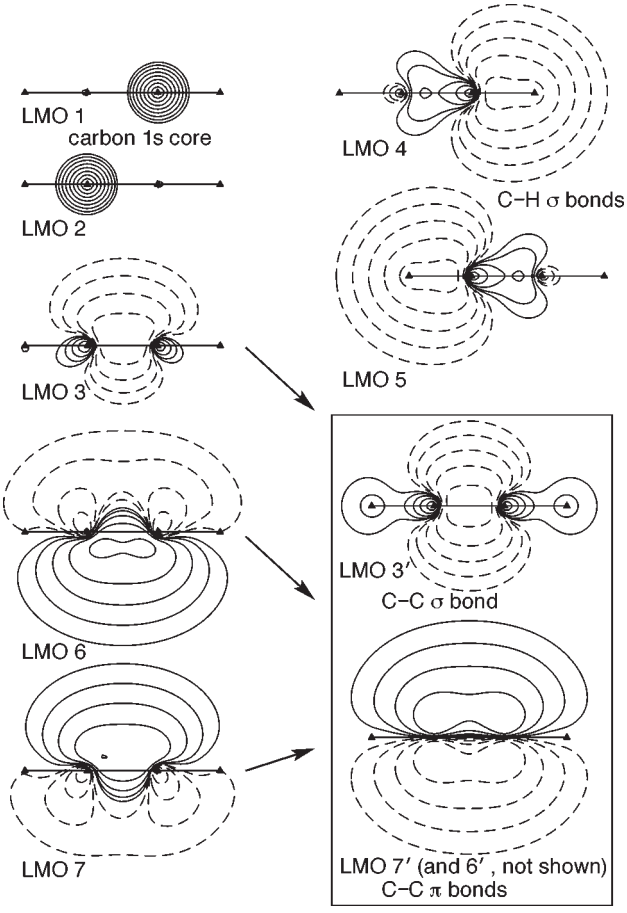

Figure 7. Localized molecular orbitals of ethyne plotted in a plane containing the C−C axis. The contour values are $\pm 0.02 \times 2^n$, n = 0, 1, 2,... $(e/a_0^3)^{1/2}$; dashed lines indicate negative values. LMOs 3, 6, and 7 are equivalent upon rotation of 120 and 240 degrees around the C−C axis. See Figure 8. LMOs 3′, 6′, and 7′ are obtained from LMOs 3, 6, and 7 by separating the σ and π contributions in the banana bonds. (6′ is not shown, equivalent to LMO 7′ but in the orthogonal plane).

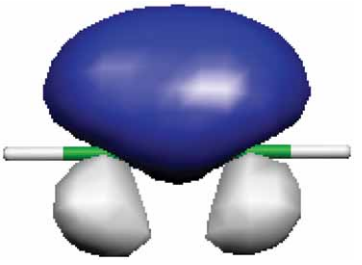

Figure 8. Three-dimensional representation of the localized molecular orbital 3 of ethyne (one of the 3 C−C "banana bonds"). The plotted isosurface value of the LMO is ± 0.060 $(e/a_0^3)^{1/2}$. LMOs 6 and 7 look the same but are rotated by 120° and 240° around the C−C axis, respectively.

Table 3. LMO Contributions to J^{FC}(C,C) in Ethyne, in Hz[a]

	LMOs							total J^{FC}
	1	2	3	4	5	6	7	
banana bonds[b]	47.2	45.9	72.9	-55.7	-53.5	72.9	72.9	202.5
σ/π[c]	38.7	36.7	219.4	-47.5	-44.8	0.0	0.0	202.5

[a]The numbers are the J_p^{FC}(A,B) of eq 11. The experimental value for the coupling is 172.7 Hz. [b]The LMOs are obtained from the entire set of MOs. They correspond to LMOs 1–7 in Figure 7. The C–C triple bond is represented by three equivalent banana bond LMOs. [c]Contributions from the set of LMOs 1′–7′ in Figure 7 in which the C–C bond is described by one σ and two π LMOs.

Table 4. FO Contributions to J^{FC}(C,C), in Hz, for Ethyne, Ethene, and Ethane

Molecule	C1		C2		H_{C1}	H_{C2}	Sum[a]	Total[b]
	1s	2s	1s	2s	1s	1s		
Ethyne	49.9	64.4	48.6	72.3	-17.4	-20.0	197.8	202.5
Ethene	18.9	25.2	14.1	33.4	-10.5	-7.7	73.4	82.7
Ethane	–	16.1	–	22.0	-7.2	-4.5	26.4	29.3

[a]Sum of listed contributions. [b]Sum of all FO contributions, equal to J^{FC}.

the absolute values of the contributions from certain equivalent LMO pairs (LMO 1 vs LMO 2; LMO 4 vs LMO 5) is a numerical artifact of the way the *J* coupling calculation is implemented efficiently.

Each banana bond has a comparatively small carbon s character. It is also possible to separate the C−C σ and π orbitals by not allowing any σ–π mixing in the localization procedure. This leads to an alternative set of LMOs 1′ to 7′ (see Figure 7). We obtain a pictorial representation of the familiar concept of two π and one σ orbitals to form the C≡C triple bond (LMOs 3′, 6′, 7′). The other σ LMOs are slightly affected by this procedure, but not to an extent that would be visible in the plots, that is, LMOs 1 and 1′; 2 and 2′; 4 and 4′; 5 and 5′, respectively, are very similar. The two π orbitals have the same LMO energy that is higher than the one of the σ C−C bonding orbital. The decomposition of *J*(C,C) in this alternative set of LMOs gives further insight into the major role played by the σ orbitals: Here we obtain a contribution of 219.4 Hz from the C−C σ bond LMO while the π LMOs do not contribute to the FC mechanism. This decomposition is perhaps closest to what one would intuitively expect for the C−C coupling: one σ C−C bonding orbital yields one large contribution that comprises most of *J*(C,C). It is reassuring that quantum theory confirms our chemical intuition: the C−C coupling is mediated by the C−C sigma bond.

Ethyne: FO Analysis of *J*(C,C)

Using the nonorthogonal orbitals of fragments that constitute the molecule (FOs) offers an alternative way of determining which orbitals are responsible for the *J* coupling. Here, we use the atomic orbitals as FOs. Table 4 lists the main FO contributions to the C−C coupling constant of ethyne. For comparison, the analyses for ethene and ethane are also listed. The dominant role in particular of the carbon 2s orbitals is obvious. The negative contributions from the C−H bonds previously seen in the LMO analysis are also present in the FO scheme in form of negative contributions from the hydrogen 1s orbitals. Again, for efficiency reasons of the *J* coupling calculations the FO decomposition yields a slight

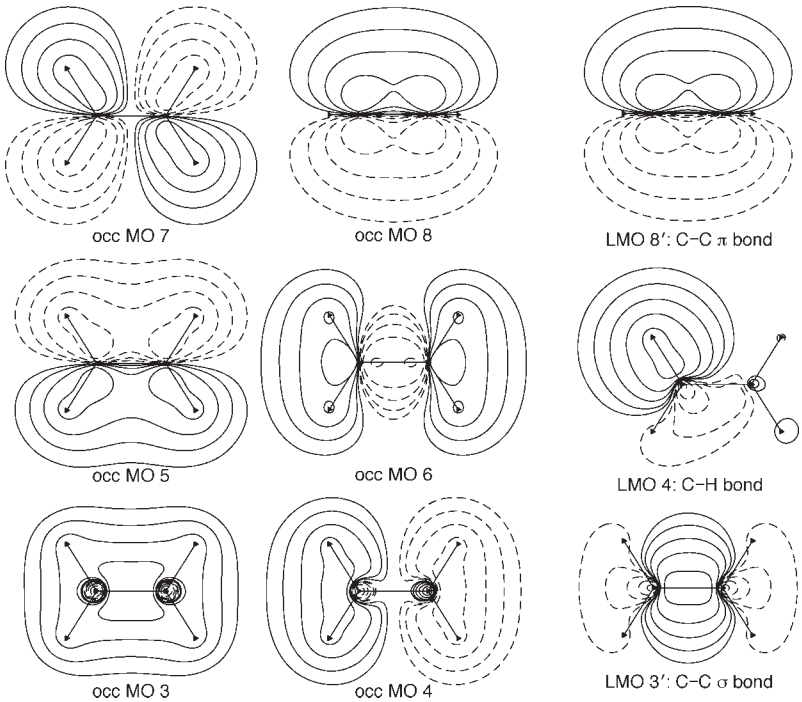

Figure 9. Selected occupied MOs (left and middle) and LMOs (right column) of ethene, plotted in the molecule's plane (except the π orbital number 8, which is plotted in the orthogonal plane containing the C−C axis). Contour values as in Figure 7. MOs 1, 2, and LMOs 1, 2, are very similar to MOs 1, 2, and LMOs 1, 2 of ethyne (carbon 1s, not shown). LMOs 5, 6, and 7 are equivalent to LMO 4 and represent the other C−H bonds. LMOs 3 and 8 are two "banana bond" LMOs for the C−C double bond. They look very similar to the ones for ethyne (Figure 8) and are not shown here. LMO 3′ represents the C−C σ bond obtained without σ–π mixing in the localization procedure, MO 8 = LMO 8′ is the corresponding C−C π bond.

Table 5. Occupied MO Contributions to J^{FC}(C,C), in Hz, According to Eq 10, for Ethyne, Ethene, and Ethane

Occ MOs	Ethyne	Ethene	Ethane
1	1311.4	958.4	631.7
2	-1318.2	-966.6	-638.4
3	425.1	253.8	162.8
4	-215.7	-165.4	-131.2
5	0.0	0.0	0.0
6	0.0	2.5	0.0
7	0.0	0.0	4.5
8		0.0	0.0
9			0.0
Total J^{FC}	202.5	82.7	29.3

NOTE: The experimental *J* couplings are 172.7, 67.8, and 34.5 Hz for ethyne, ethene, and ethane, respectively,

Table 6. LMO Contributions to J^{FC}(C,C), in Hz, according to Eq 11, for Ethene and Ethane

LMOs	Ethene		Ethane[c]
	banana[a]	σ/π[b]	
1	20.3	17.5	5.8
2	15.6	12.5	1.1
3	55.5	106.7	-6.6
4	-16.8	-14.5	-6.6
5	-16.8	-14.5	-6.6
6	-15.2	-12.5	-6.6
7	-15.2	-12.5	58.9
8	55.5	0.0	-5.6
9	–	–	-5.6
Total J^{FC}	82.7	82.7	29.3

[a]The C–C double bond is described by two "banana bond" LMOs 3 and 8. [b]The C–C double bond is described by a σ–bond LMO 3′ and a π–bond LMO 8′. [c]The C–C single bond is represented by LMO 7. The experimental *J* couplings are 67.8 and 34.5 Hz for ethene and ethane, respectively.

dissymmetry in contributions from equivalent FOs, but not to an extent that would obscure the analysis.

It is surprising that the 1s carbon core orbitals show such large contributions for ethene and ethyne. However, they reflect the contributions from the core–valence orthogonality that also emerged in the other decompositions. Our data indicate that these contributions are large for the short C−C distance in the triple bond.

Summary for Ethyne

The main conclusions from the analysis of J^{FC}(C,C) in ethyne are:

- The different decomposition schemes (canonical MOs, LMOs, FOs) yield similar interpretations. The *J* coupling is governed mainly by the s valence orbitals of the atoms directly involved in the bond and negative contributions from other atoms bound to them. *J* coupling can be considered as a valence property (i.e., a "chemical" property).
- The orthogonality of MOs (localized or not) yields additional, "orthogonality contributions" from orbitals that do not directly participate in the bonding (core MOs, bonds between other atoms). This is also reflected in the FO analysis.
- The LMO decomposition appears to be most intuitive to describe *J* couplings. The LMOs also most intuitively depict the bonds in the molecule.
- The bonding–antibonding pattern of the canonical σ MOs is clearly related to the sign of the *J*-coupling contributions.

Ethane and Ethene: Analysis of J(C,C)

By comparing the results of ethyne with ethane and ethene we can now analyze the trends for the C−C *J* couplings with increasing C−C bond distances and for different carbon hybridizations. *J*(C,C) is strongly decreasing from ethyne to ethene and ethane (see Table 1).

The canonical occupied MOs and some LMOs of ethene and ethane are shown in Figures 9 and 10, respectively. The *J* coupling contributions from the occupied MOs and the LMOs are compared in Tables 5 and 6, respectively. Based

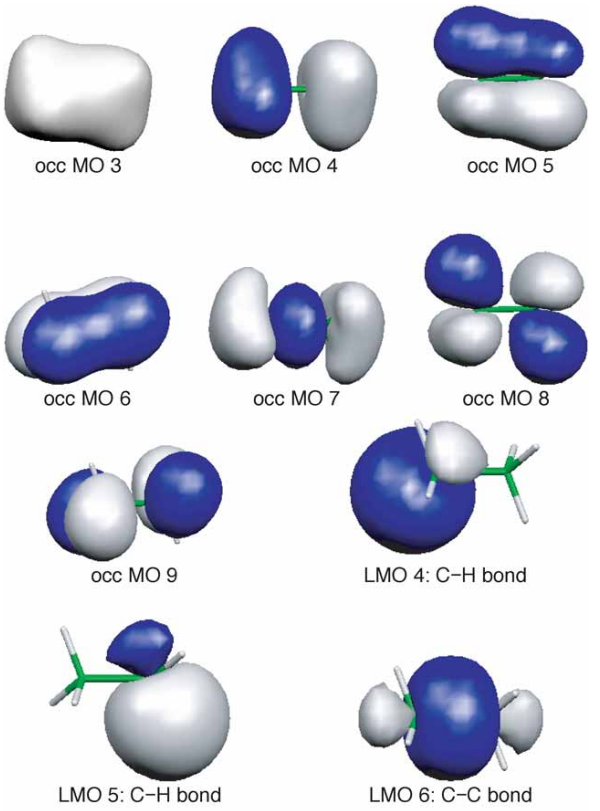

Figure 10. 3D plots of selected occupied MOs and LMOs of ethane. Isosurface values are ±0.035 $(e/a_0^3)^{1/2}$. The MOs 1, 2 and LMOs 1, 2 (not shown) are similar to MOs 1, 2, and LMOs 1, 2 of ethyne, respectively. LMOs 3 and 6 and LMOs 8 and 9 (C−H bonds, not shown) are equivalent to LMOs 5 and 4, respectively, but rotated by 120° and 240°. LMO 7 represents the C−C single bond.

on the MO analysis, the conclusions obtained for ethyne can be extended to ethene and ethane. The carbon core 1s MOs 1 and 2 yield huge, but noticeably smaller, contributions to J^{FC}(C,C) than for ethyne. As for ethyne, these contributions mutually cancel. The decrease of J^{FC}(C,C) is thus explained by the simultaneous decrease of the positive contribution of the 2s–σ bonding orbital (MO 3) and of the negative contribution of its antibonding analog (MO 4). The LMO analysis identifies one C−C bonding σ LMO instead that yields most of the total coupling. Both the change of carbon hybridization and the increase of the C−C distance are responsible for the observed trend of decreasing J^{FC}(C,C). Suppose the FC contributions to the C−C *J* couplings were only governed by the carbon s character and not by the C−C distance, we might expect ratios of 4:(16/9):1 ≈ 4:1.8:1 for J^{FC} in ethyne/ethene/ethane. The ratios are obtained by multiplying the carbon s-characters for sp (½·½) in ethyne, sp^2 (⅓·⅓) in ethene, and sp^3 (¼·¼) hybridized carbon atoms in ethane. Obviously, J^{FC}(C,C) decreases more strongly than these ratios. From the calculations, we obtain 6.9:2.8:1 instead. This shows that the C−C distances affect the *J* couplings quite significantly. The shorter the bond, the larger *J*(C,C) for this series of molecules. In summary, both the carbon hybridization as well as the C−C distances have a major influence on the FC mechanism of the *J* couplings.

Benzene: Analysis of J(C,H)

As we have seen for ethyne, ethene, and ethane, it is difficult to separate in the trend of *J*(C,C) the influences of the C−C distance and the carbon hybridization. Additional information can be gathered by considering the C−H one-bond *J* couplings (see Table 1). Indeed, the experimental C−H bond distances remain very similar in ethyne, ethene, and ethane and the C−H *J* couplings might thus depend mainly on the carbon hybridization. For this series of hydrocarbons, the empirical Muller–Pritchard relationship relates the one-bond *J*(C,H) to the s character of the hybrid orbital that forms the C−H bond *(45, 46)*:

$$J(\mathrm{C,H}) \approx a_{\mathrm{CH}} s_{\mathrm{C}} s_{\mathrm{H}} - b_{\mathrm{CH}} \qquad (13)$$

Here, s_H and s_C are the hydrogen and carbon s character, respectively. a_{CH} and b_{CH} are empirical constants. By setting the s character s_H equal to 1 and the constant b_{CH} to zero, the following simpler relation was derived from the experimental values for the one-bond couplings *(45)*:

$$J(\mathrm{C,H}) \approx 500\,\mathrm{Hz} \cdot s_{\mathrm{C}} \qquad (14)$$

According to this equation, for an sp^3-hybridized carbon atom (s_C = 0.25), *J*(C,H) will be around 125 Hz, and for sp^2- and sp-hybridized carbon atoms, ^1J(C,H) will be about 167 and 250 Hz, respectively (s_C = 0.3, 0.5). The experimental data for ethane, ethene, and ethyne as well as the computational results agree well with these estimates. With an experimental *J*(C,H) of 157.7 Hz, benzene also agrees well with this rule with an assumed sp^2-hybridization for the carbon atoms. The C−H coupling is almost identical to the one in ethene, which also has sp^2-hybridized carbons. However, ^1J(C,C) for benzene (56.2 Hz) is noticeably different than for ethene (67.8 Hz). Similar trends are found in the computations. This difference is due to the larger C−C distance in benzene (1.40 Å vs 1.34 Å in ethene), driven by the delocalization of the π system in this molecule. This delocalization can be pictorially represented by LMOs (Figure 11). Whereas the C−H and C−C σ LMOs are two-center orbitals, the π LMOs are four-center orbitals with large orthogonalization tails. The multicenter character of these π LMOs reflects the delocalization of the π system.

Within typical ranges of bond distances, *J* coupling often decreases exponentially with increasing internuclear distance. Let us try if the C−C bond distance in benzene can be estimated from its C−C coupling constant by assuming a simple exponential relation. First, we fit

$$\ln\left[J(\mathrm{C,C})/\mathrm{Hz}\right] \approx a + bR \qquad (15)$$

using the experimental bond lengths (*R*) and coupling constants of ethyne, ethene, and ethane. The parameters *a* and *b* are found to be 10.741 and −4.736 $Å^{-1}$, respectively. If we use the fit parameters along with the experimental *J*(C,C) of benzene (56.2 Hz), the estimated C−C bond length is 1.417 Å, which is reasonably close to the measured distance (1.397 Å).

The SD and PSO Terms

Here, we summarize some of the insights into the nature of the C−C bond that were recently gained from studying the SD and PSO mechanisms *(13, 15–17)*. What needs to be known is that the PSO operator behaves like an angular momentum operator (see eq 30 in the Appendix in the Supplemental Material[W]). Therefore, in the case of C−C bonding the PSO mechanism involves both p_σ and p_π orbitals. In the SD mechanism, only the p_π orbitals are involved.

The SD and PSO terms are both dependent on the multiple bond character of the C−C bond (Table 7). In the series ethane, ethene and ethyne, both SD and PSO terms increase in magnitude with increasing C−C bond order. It has been suggested that the absolute value of the sum SD + PSO reflects the increasing π-character of the C−C bond in this set of molecules *(13)*. For benzene, this sum lies in between the values for ethene and ethane, reflecting the mixed single–double bond character of the C−C bonds. As an example for the role of the 2p AOs in the PSO term, we discuss the case of ethyne with the help of the canonical MO contributions. An analysis shows that MOs 5 (p_σ, −10.2 Hz), 6, and 7 (p_π, 7.7 Hz) yield the main contributions to the PSO term, owing to the mixing with the vacant π MOs 8 and 9 (LUMOs). The different signs of the PSO contributions can be explained in a similar pictorial way as for the FC coupling (see Figure 6), but by taking into account the action of the angular momentum operator on the p-type orbitals (which results in a rotation of the orbital by 90° around the axis of the operation). For details we refer to ref *47*.

Coupling Through More Than One Bond

So far we have considered only one–bond couplings. They are the easiest to analyze computationally. However, the equations, computational approach, and orbital analysis methods shown previously can be applied to two-bond (geminal, ^2J) and three-bond (vicinal, ^3J) coupling constants as well. Both generally display a strong dependence on the molecular geometry. Perhaps best known is the *Karplus relation-*

ship for three-bond H−H couplings *(48)*. For ethane derivatives, the following approximate dependence of ^3J(H−H) on the HCCH dihedral angle ϕ was obtained from theoretical considerations

$$^3J = A + B\cos\phi + C\cos 2\phi \qquad (16)$$

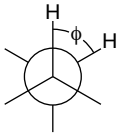

with A, B, C having values of approximately 4.22, −0.5, and 4.5 Hz, respectively. Other authors have suggested empirical values of A = 7, B = −1, C = 5 Hz, which yield better overall agreement with experimental data *(26)*. The Karplus relation has been very useful to distinguish, for example, between cis and trans isomers of the same compound by NMR. For a computational exercise, students can easily determine $^3J(\phi)$ numerically for ethane for a range of dihedral angles ϕ and fit the data to eq 16. The free software "gnuplot" *(49)* can be used for the data fitting procedure. The results might then be used by the students to assign a set of cis–trans isomer pairs such as shown in Günther's textbook (*26,* p 116) with the help of ^3J data.

Finally, we would like to point out that in many cases the sign pattern of ^1J, ^2J, ^3J in a molecule alternates. An example is ethane where, as seen previously, ^1J(C,C) and ^1J(C,H) are positive (Table 1). ^2J(C,H), on the other hand, is negative (−4.7 Hz), and ^3J(H,H) is positive (8.0 Hz). For experimental values see ref *50*. The sign pattern is related to the induced spin polarization in the electronic system as indicated in Figures 3 and 6. As we have seen, products of an occupied with vacant σ orbitals must have opposite sign at the two nuclei for the J contributions to be positive (the FC term, to be precise). Alternatively, we may say: The induced spin polarization has to be of different sign at the two nuclei. If we consider a system of 3 nuclei A–B–C where the induced spin polarization from, say, nucleus A has the sign pattern −/+/− then ^1J(A,B) > 0 but ^1J(A,C) < 0. This appears to be the case in ethane. On the other hand, the coupling constants in ethyne are all positive, that is, the sign alternation is not observed *(50)*. For an illustration, we plot the spin polarization for the two systems in Figure 12 where one of the carbons is considered as the nucleus that induces the spin polarization. It can be seen that the sign change pattern is indeed the expected one.

Table 7. Calculated Spin–Dipole (SD) and Paramagnetic (PSO) Contributions to the *J* Couplings, in Hz

Molecule	C_2H_2	C_2H_4	C_2H_6	C_6H_6
SD	8.0	2.2	0.9	0.7
PSO	6.1	-9.3	-0.1	-6.5
SD + PSO	14.1	-7.1	0.8	-5.8

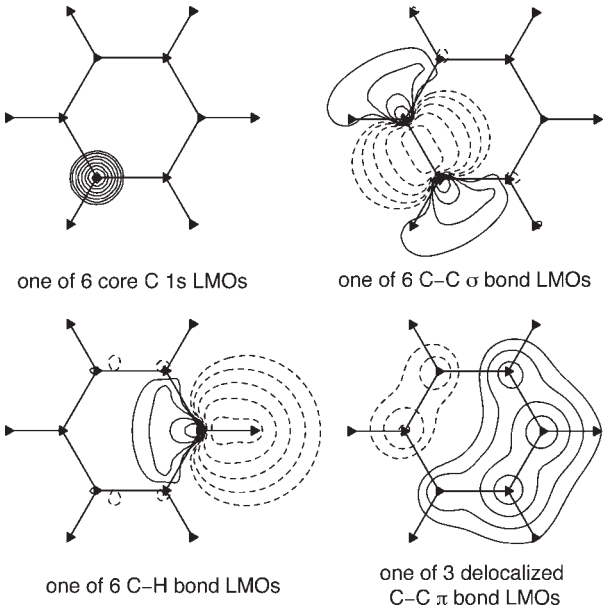

Figure 11. Some localized molecular orbitals of benzene. σ LMOs are plotted in the plane of the molecule. The π LMO is plotted 0.5 Å above the molecular plane. Contour values as in Figure 7.

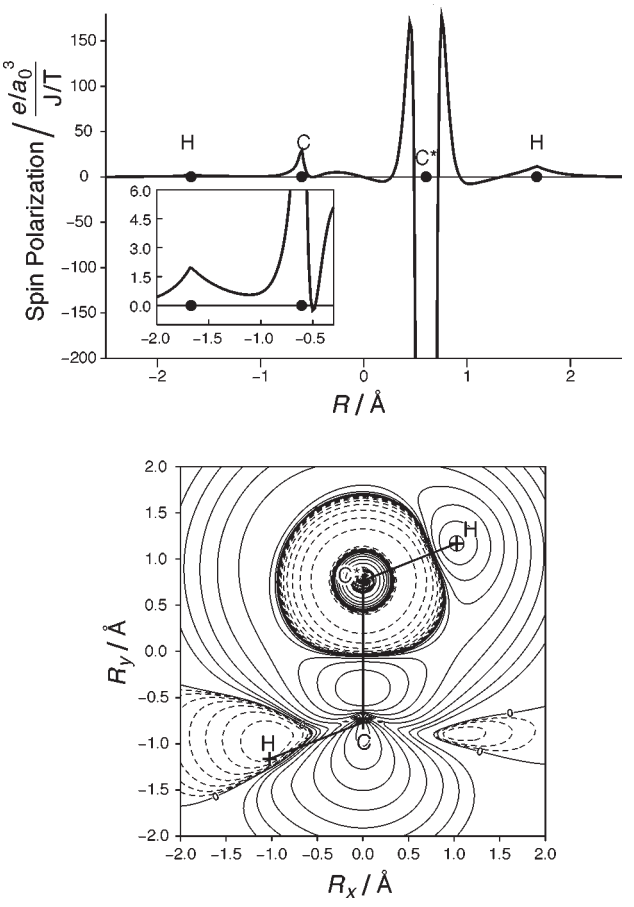

Figure 12. Induced spin polarization per unit magnitude of a perturbing nuclear spin magnetic moment of one of the carbons (indicated as C*) in ethyne (top) and ethane (bottom). Top: Plot along the molecular axis. Bottom: Plot in a plane containing the C−C axis and two of the C−H bonds. The spin polarization at C* is negative.

Conclusion

First-principles calculations and orbital-based analyses of *J* couplings can be useful to emphasize the relations between the nature of a chemical bond and observable properties that probe this bond. We have found that assignments based on the material presented here provide a valuable "hands-on" experience for students who want to learn about the origin of NMR spin–spin coupling. From our experience, students easily accept the concept of "contributions to molecular properties from individual orbitals" without the need to provide explicit equations. By using the theoretical formalism, further insight into *J* coupling mechanisms may be gained.

Acknowledgments

This work has received financial support from the CAREER program of the National Science Foundation (CHE-0447321). Special thanks to undergraduate student M. E. Pragel who performed many of the calculations shown in this article, to Eva Zurek for careful proofreading of the manuscript, and to Mariusz Sterzel for preparing Figure 12. We also thank the students who participated in the course where the material was first used. Finally, we are grateful for the constructive comments from the referees.

[W]Supplemental Material

Quantum theory of *J* coupling and some additional formulas and supporting information are available in this issue of *JCE Online*.

Notes

1. Usually, the term "current density" is used in this context but we will keep using the word "current" for reasons of simplicity.

2. In principle, we should write:

$$\mathbf{B}^{\text{local}} = \left(\{\mathbf{1}\} - \boldsymbol{\sigma}_{\text{A}}\right)\mathbf{B}^{\text{ext}}$$

where $\boldsymbol{\sigma}_{\text{A}}$ is a rank-2 tensor, similar to the coupling tensors in eq 3, and $\{\mathbf{1}\}$ is the unit matrix of rank 2. In the text we use a notation for the magnitudes in order to keep the notation simple.

3. The correct technical term to be used here would be *electron spin density,* but we will keep using the phrase "spin polarization".

4. As stated before, we base our discussion on a theoretical model where in the ground state the molecular orbitals are fully occupied, and vacant orbitals have zero occupation (Hartree–Fock, DFT, semiempirical methods). More generally, in correlated ab–initio theoretical methods, one can describe the electron density with an (in principle infinite) set of molecular orbitals with non-integer occupations. This electronic structure undergoes a change in the presence of a nuclear spin that can be conceptually understood by the change in occupancy of these orbitals. The clearcut occupied–vacant orbital situation is a special case.

5. A somewhat more sloppy formulation would be: A fraction of electrons move into higher lying orbitals.

6. Each orbital also carries a spin factor of alpha = (1,0) or beta = (0,1) on which the spin operator $\hat{S}_z$ acts.

Literature Cited

1. Bryce, D. L.; Wasylishen, R. E. *J. Chem. Educ.* **2001,** *78,* 124–133.
2. Tilley, L. J.; Prevoir, S. J.; Forsyth, D. A. *J. Chem. Educ.* **2002,** *79,* 593–600.
3. Kowalewski, J. *Annu. Rep. NMR Spectrosc.* **1982,** *12,* 81–176.
4. Contreras, R. H.; Peralta, J. E.; Giribet, C. G. *Annu. Rep. NMR Spectrosc.* **2000,** *41,* 55–184.
5. Facelli, J. C. Shielding Calculations. In *Encyclopedia of Nuclear Magnetic Resonance;* Grant, D. M., Harris, R. K., Eds.; John Wiley & Sons: Chichester, United Kingdom, 2002; Vol. 9.
6. Fleischer, U.; van Wüllen, C.; Kutzelnigg, W. NMR Chemical Shift Computation: Ab Initio. In *Encyclopedia of Computational Chemistry;* von Ragué Schleyer, P., Ed.; John Wiley & Sons: Chichester, United Kingdom, 1998.
7. Bühl, M.; Kaupp, M.; Malkina, O. L.; Malkin, V. G. *J. Comput. Chem.* **1999,** *20,* 91–105.
8. Helgaker, T.; Jaszunski, M.; Ruud, K. *Chem. Rev.* **1999,** *99,* 293–352.
9. Autschbach, J.; Ziegler, T. Relativistic Computation of NMR Shieldings and Spin–Spin Coupling Constants. In *Encyclopedia of Nuclear Magnetic Resonance;* Grant, D. M., Harris, R. K., Eds.; John Wiley & Sons: Chichester, United Kingdom, 2002; Vol. 9.
10. Autschbach, J. The Calculation of NMR Parameters in Transition Metal Complexes. In *Principles and Applications of Density Functional Theory in Inorganic Chemistry I;* Kaltsoyannis, N., McGrady, J. E., Eds.; Springer: Heidelberg, Germany, 2004; Vol. 112.
11. *Calculation of NMR and EPR Parameters—Theory and Applications;* Kaupp, M.; Bühl, M.; Malkin, V. G., Eds.; Wiley-VCH: Weinheim, Germany, 2004.
12. Wu, A.; Graefenstein, J.; Cremer, D. *J. Phys. Chem. A* **2003,** *107,* 7043–7056.
13. Cremer, D.; Kraka, E.; Wu, A.; Lüttke, W. *Chem. Phys. Chem.* **2004,** *5,* 349–366.
14. Gräfenstein, J.; Tuttle, T.; Cremer, D. *J. Chem. Phys.* **2004,** *120,* 9952–9968.
15. Gräfenstein, J.; Cremer, D. *Chem. Phys. Lett.* **2004,** *383,* 332–342.
16. Gräfenstein, J.; Cremer, D. *Chem. Phys. Lett.* **2004,** *387,* 415–427.
17. Gräfenstein, J.; Kraka, E.; Cremer, D. *J. Phys. Chem. A* **2004,** *108,* 4520–4535.
18. Autschbach, J.; Ziegler, T. *J. Am. Chem. Soc.* **2001,** *123,* 3341–3349.
19. Autschbach, J.; Ziegler, T. *J. Am. Chem. Soc.* **2001,** *123,* 5320–5324.
20. Autschbach, J.; Igna, C. D.; Ziegler, T. *J. Am. Chem. Soc.* **2003,** *125,* 1028–1032.
21. Autschbach, J.; Le Guennic, B. *J. Am. Chem. Soc.* **2003,** *125,* 13585–13593.
22. Le Guennic, B.; Matsumoto, K.; Autschbach, J. *Magn. Reson. Chem.* **2004,** *42,* S99–S116.
23. McWeeny, R. *Methods of Molecular Quantum Mechanics,* 2nd ed.; Academic Press: London, 1992.
24. Atkins, P. W.; Friedman, R. S. *Molecular Quantum Mechanics;* Oxford University Press: New York, 1997.

25. Wasylishen, R. Dipolar and Indirect Coupling Tensors in Solids. In *Encyclopedia of Nuclear Magnetic Resonance;* Grant, D. M., Harris, R. K., Eds.; John Wiley & Sons: Chichester, United Kingdom, 1996.
26. Günther, H. *NMR Spectroscopy,* 2nd ed.; John Wiley & Sons: Chichester, United Kingdom, 1995.
27. Bryce, D. L.; Wasylishen, R. E.; Autschbach, J.; Ziegler, T. *J. Am. Chem. Soc.* **2002,** *124,* 4894–4900.
28. Boys, S. F.; Foster, J. M. *Rev. Mod. Phys.* **1960,** *32,* 300–302.
29. Boys, S. F. In *Quantum Theory of Atoms, Molecules and the Solid State;* Löwdin, P. O., Ed.; Academic Press: New York, 1966.
30. Frisch, M. J.; et al. *Gaussian 03;* Gaussian, Inc.: Wallingford, CT, 2004; *http://www.gaussian.com* (accessed Oct 2006).
31. Baerends, E. J.; et al. *Amsterdam Density Functional* (ADF); Scientific Computing & Modeling: Amsterdam, 2005; Vrije Universiteit, Theoretical Chemistry; *http://www.scm.com* (accessed Oct 2006).
32. Glendening, E. D.; Badenhoop, J. K.; Reed, A. E.; Carpenter, J. E.; Bohmann, J. A.; Morales, C. M.; Weinhold, F. *NBO 5.0;* Theoretical Chemistry Institute, University of Wisconsin–Madison: Madison, WI, 2001; *http://www.chem.wisc.edu/~nbo5* (accessed Oct 2006).
33. National Institute of Standards and Technology. Computational Chemistry Comparison and Benchmark DataBase. *http://srdata.nist.gov/cccbdb* (accessed Oct 2006).
34. Fonseca Guerra, C.; Visser, O.; Snijders, J. G.; te Velde, G.; Baerends, E. J. Parallelization of the Amsterdam Density Functional Program. In *Methods and Techniques for Computational Chemistry;* STEF: Cagliari, Sardinia, Italy, 1995.
35. te Velde, G.; Bickelhaupt, F. M.; Baerends, E. J.; van Gisbergen, S. J. A.; Fonseca Guerra, C.; Snijders, J. G.; Ziegler, T. *J. Comput. Chem.* **2001,** *22,* 931–967.
36. Documentation for the options to be used for spin–spin calculations is available in the instructions for the "CPL" module at *http://www.scm.com* (accessed Oct 2006).
37. Autschbach, J.; Ziegler, T. *J. Chem. Phys.* **2000,** *113,* 936–947.
38. Autschbach, J.; Ziegler, T. *J. Chem. Phys.* **2000,** *113,* 9410–9418.
39. Flükiger, P.; Lüthi, H. P.; Portmann, S.; Weber, J. *MOLEKEL,* version 4.3; Swiss Center for Scientific Computing: Manno, Switzerland, 2000–2002.
40. Author's Web site. *http://www.nsm.buffalo.edu/~jochena/downloads/downloads.html* (accessed Oct 2006).
41. Shaftenaar, G. *Molden: A Pre- and Post-Processing Program of Molecular and Electronic Strucutre,* version 4.4; Centre for Molecular and Biomolecular Informatics, Radboud University: Nijmegen, The Netherlands; *http://www.cmbi.kun.nl/~schaft/molden/molden.html* (accessed Oct 2006).
42. *GOpenMol,* version 3.0; CSC—Scientific Computing Ltd.: Espoo, Finland, 2005; *http://www.csc.fi/gopenmol* (accessed Oct 2006).
43. Becke, A. D. *Phys. Rev. A* **1988,** *38,* 3098–3100.
44. Perdew, J. P. *Phys. Rev. B* **1986,** *33,* 8822–8824.
45. Muller, N.; Pritchard, D. E. *J. Chem. Phys.* **1959,** *31,* 768–771.
46. Newton, M. D.; Schulman, J. M.; Manus, M. M. *J. Am. Chem. Soc.* **1974,** *96,* 17–23.
47. Wiberg, K. B.; Hammer, J. D.; Zilm, K. W.; Cheeseman, J. R. *J. Org. Chem.* **1999,** *64,* 6394–6400.
48. Karplus, M. *J. Am. Chem. Soc.* **1963,** *85,* 2870–2871.
49. Gnuplot Home Page. *http://www.gnuplot.info* (accessed Oct 2006).
50. Kaski, J.; Lantto, P.; Vaara, J.; Jokisaari, J. *J. Am. Chem. Soc.* **1998,** *120,* 3993–4005.